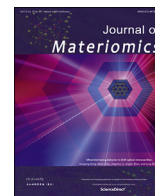




Contents lists available at ScienceDirect

Journal of Materiomics

journal homepage: www.journals.elsevier.com/journal-of-materiomics/

Tailoring microstructure and electrical transportation through tensile stress in Bi₂Te₃ thermoelectric fibers

Min Sun^{a,b}, Guowu Tang^{a,b}, Bowen Huang^b, Zhongjia Chen^a, Yu-Jun Zhao^a, Hanfu Wang^c, Ziwen Zhao^d, Dongdan Chen^b, Qi Qian^{b,*}, Zhongmin Yang^{a,b,**}

^a School of Physics and Optoelectronics, South China University of Technology, Guangzhou, 510640, China

^b State Key Laboratory of Luminescent Materials and Devices, Institute of Optical Communication Materials, Guangdong Engineering Technology Research and Development Center of Special Optical Fiber Materials and Devices, Guangdong Provincial Key Laboratory of Fiber Laser Material and Applied Techniques, South China University of Technology, Guangzhou, 510640, China

^c CAS Key Laboratory of Nanosystem and Hierarchical Fabrication, National Center for Nanoscience and Technology of China, Beijing, 100190, China

^d Key Laboratory of Specialty Fiber Optics and Optical Access Networks, Shanghai Institute for Advanced Communication and Data Science, School of Communication and Information Engineering, Shanghai University, Shanghai, 200072, China

ARTICLE INFO

Article history:

Received 11 September 2019

Received in revised form

15 January 2020

Accepted 7 February 2020

Available online 10 February 2020

Keywords:

Bi₂Te₃

Thermoelectric fiber

Tensile stress

Electrical transportation

ABSTRACT

Bismuth telluride (Bi₂Te₃) has attracted much attention in the field of thermoelectrics since it is one kind of commercial room-temperature thermoelectric material. Herein three kinds of Bi₂Te₃ thermoelectric fibers with internal tensile stress are fabricated utilizing an optical fiber template method. The effects of internal stress on the microstructure and the electrical transportation of Bi₂Te₃ thermoelectric fibers are investigated. The Bi₂Te₃ cores in the fibers are highly crystalline and possess a tensile nanosheet structure with preferential orientation as evidenced by X-ray diffraction and Raman studies. Tensile stress can enhance electrical properties of the fibers. And a paper cup generator covered with 20 pieces of optimized fibers provides a μW-level output power. It is inferred that tensile stress tuning can be an effective tool for the material optimization of thermoelectric performance.

© 2020 The Chinese Ceramic Society. Production and hosting by Elsevier B.V. This is an open access article under the CC BY-NC-ND license (<http://creativecommons.org/licenses/by-nc-nd/4.0/>).

1. Introduction

Thermoelectric (TE) materials, having capability to convert energy between heat and electricity, are critical materials for effective waste heat recovery and compact refrigeration systems [1–3]. It is a huge challenge to substantially improve TE materials properties, even though doped Bi₂Te₃ crystals with 2.4 ZT value, dimensionless thermoelectric figure of merit, have been reported to be the best room-temperature TE materials so far ($ZT = S^2\sigma/T\kappa$, where S is Seebeck coefficient, σ is electrical conductivity, T is absolute temperature and κ is thermal conductivity) [4–9]. It has been found

that applying pressure stress to materials permits significantly changing the relevant properties of materials, for example, band-gaps tuning [10–12]. Pressure stress effects on the main TE properties of Bi₂Te₃, such as power factor ($PF=S^2\sigma$) and ZT , have been studied in some works [13–16]. It was proved that a pressure over 6 GPa induces a phase transition of Bi₂Te₃, from a rhombohedral phase to a monoclinic phase [17–20], illustrating that a compressive stress could modulate crystal structure. Logically, it can be expected how a tensile stress adjust the structure of a crystal, following changes of its properties. However, it is relatively difficult to apply tensile stress on a crystal as it crystallizes from the melt.

Here, we investigate tensile stress effects on the course of Bi₂Te₃ crystallizing. The tensile stress comes from the conventional optical fiber configuration, in which Bi₂Te₃ and glasses are selected as the core and the cladding of the fibers, respectively. It is demonstrated that high tensile stress can adjust the Bi₂Te₃ structure and greatly enhance the PF of Bi₂Te₃ fiber core. And the fibers are further utilized to construct an efficient TE fiber cup generator. We propose a mechanism of the tension-driven enhancement of TE performance, which will be important for future development of broad functional material systems.

* Corresponding author.

** Corresponding author. State Key Laboratory of Luminescent Materials and Devices, Institute of Optical Communication Materials, Guangdong Engineering Technology Research and Development Center of Special Optical Fiber Materials and Devices, Guangdong Provincial Key Laboratory of Fiber Laser Material and Applied Techniques, South China University of Technology, Guangzhou, 510640, China.

E-mail addresses: qianqi@scut.edu.cn (Q. Qian), yangzm@scut.edu.cn (Z. Yang).

Peer review under responsibility of The Chinese Ceramic Society.

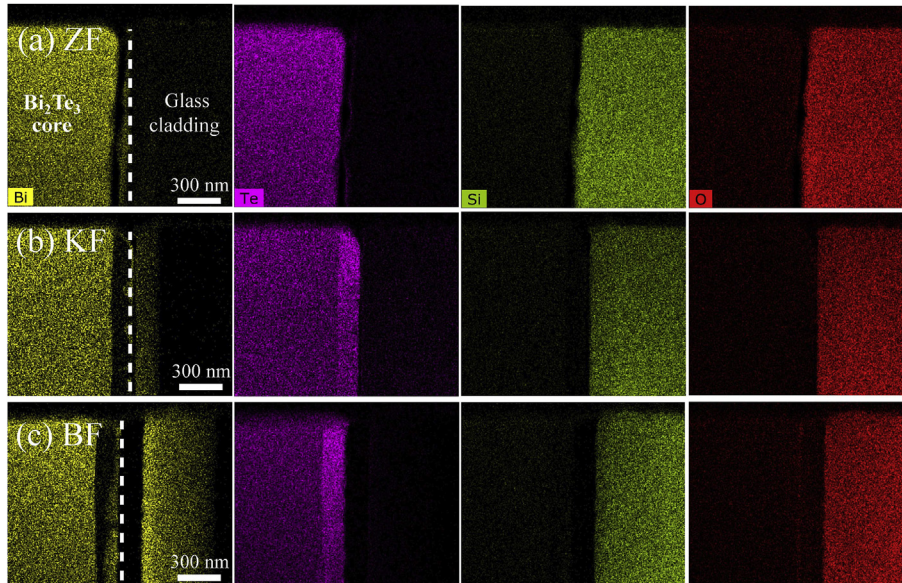


Fig. 1. EDS elemental mappings in the chip sample of (a) ZF, (b) KF, and (c) BF fibers.

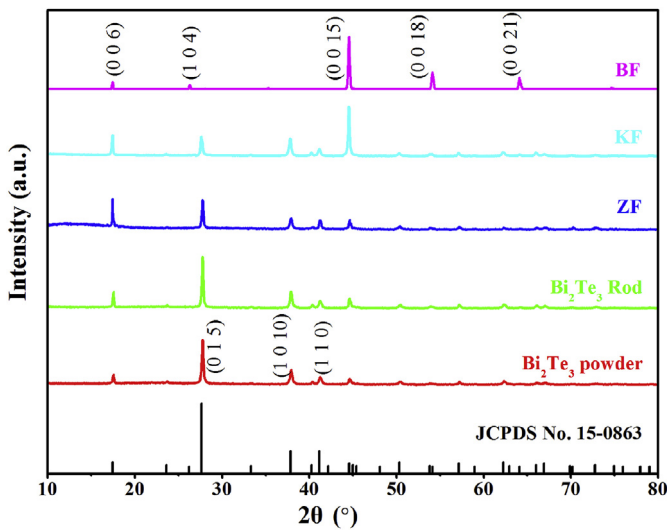


Fig. 2. XRD patterns of the Bi_2Te_3 powder, rod, and three Bi_2Te_3 cores.

2. Material and methods

2.1. Samples preparation

In this work, the rod-in-tube technique was used for fabricating composite Bi_2Te_3 TE fibers with Bi_2Te_3 crystalline core and glass claddings. Bi_2Te_3 raw powders of 99.99% purity (under 200 mesh, Aladdin Industrial) were molten, then hardened into shape in a quartz tube to obtain dense Bi_2Te_3 rods as the core of fiber preform, and the detailed fabrication method of undoped Bi_2Te_3 rods was same as a previous study [21]. To fabricate Bi_2Te_3 -core glass-clad fibers, the lead silicate (ZF3), alkali silicate (K9), and borosilicate (Pyrex3.3) glass tubes (Nantong Zhenhua Optical-electric Corporation) were chosen as the fiber cladding, given their suitable fiber-drawing properties and different thermal expansion coefficients. Three obtained Bi_2Te_3 rods with 3-mm-outer diameter were

Table 1

Basic physical properties of Bi_2Te_3 , ZF3, K9, and Pyrex3.3 glass.

Bi_2Te_3	ZF3	K9	Pyrex3.3	
Melting point T_m (°C)	585	/	/	/
Glass transition point T_g (°C)	/	424	555	520
Softening point T_f (°C)	/	480	630	820
Volume density ρ (g/mL)	7.58	4.2	2.49	2.23
Thermal expansion coefficient α ($10^{-6}/\text{K}$)	17	8.8	7	3.3

respectively inserted into three glass tubes of ZF3, K9, and Pyrex3.3 with 3-mm-inner and 30-mm-outer diameter, which were closed at one end and possessed different soft temperature of 480 °C, 630 °C, and 820 °C, respectively. Then the other end of each tube was evacuated and thermally sealed under 10^{-3} Pa to form three fiber preforms. Three kinds of meter-long Bi_2Te_3 TE fibers were drawn at approximately 660 °C, 840 °C, and 950 °C, respectively, using an optical fiber drawing tower. Moreover, the ZF3, K9, and Pyrex3.3 glass-clad TE fibers with an inner diameter of 50 ± 5 μm are marked as ZF, KF, and BF.

2.2. Measurements

The crystalline phase of the pure fibrous cores was identified by an X-ray powder diffractometer (X'Pert PROX, Cu $K\alpha$). Three microchip samples at the core-clad interfaces of fibers were obtained for analyzing their element distribution and microstructure, using the focused ion beam (FIB, FEI Helios 450s). FIB was operated at 30 kV starting voltage of the ion beam for initial thinning until sample thickness reached less than several micrometers and then 5 kV accelerating voltage was used for final thinning. High-resolution transmission electron microscopy (HR-TEM) measurements were performed using a transmission electron microscope (FEI Titan Themis 200) with a high angle annular dark field (HAADF) detector. The cross-section of the TE fibers was observed by a field electron-scanning electron microscope (FE-SEM, ZEISS Merlin). TEM was operated at 200 kV and SEM was operated at 20 kV. Raman spectra were collected on the polished cross-section

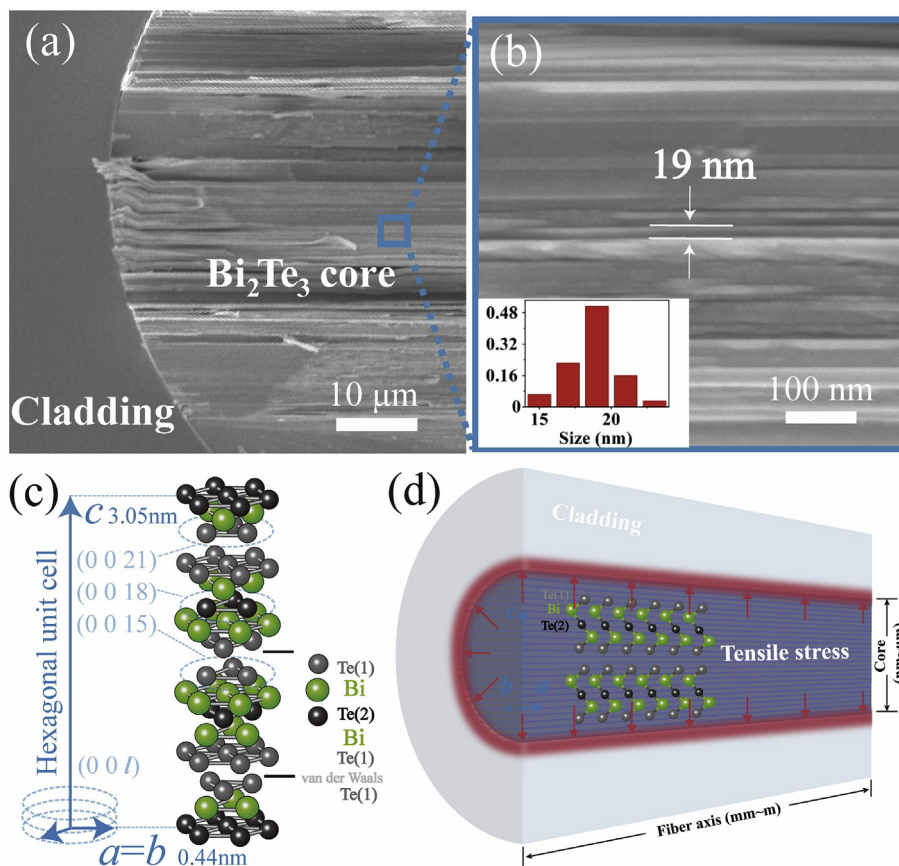


Fig. 3. (a) Scanning electron micrograph of the BF core cross-section, and (b) high-magnification image of the boxed region in (a), with the inset in (b): a summary of sheet thickness; (c) Structural model of a Bi₂Te₃ hexagonal unit cell; (d) Schematic diagram of tensile stress in the fiber core.

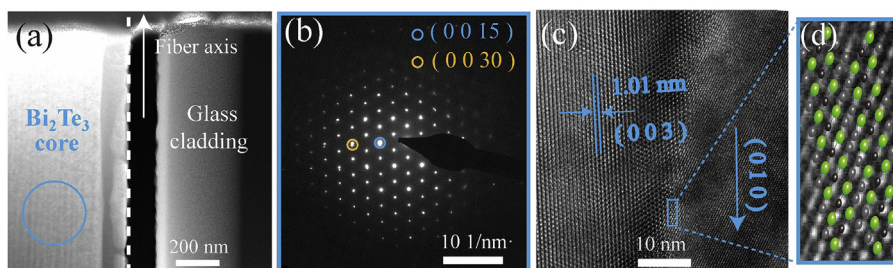


Fig. 4. (a) HAADF image of a BF chip sample and (b) SAED pattern of the circled region in (a); (c) HR-TEM image of the BF core and (d) enlarged view of the boxed region in (c).

of Bi₂Te₃ core in the backscattering configuration excited by 633 nm using a Raman spectrometer (LabRam HR-Evolution, Horiba Jobin Yvon).

Several TE fibers were cut from the as-drawn fibers. Two ends of the fibers were coated with 20-nm-thickness platinum thin films by vacuum sputtering and were attached with silver wires through silver paste for measuring electrical conductivity. To measure the seebeck coefficient, one end of the fibers was heated by a heater (TC038-PC, HC Photonics) and the other end contacted with a heat sink. The generated TE voltage ΔU of the fibers were obtained by a digital source meter (Keithley 2450), while the temperature difference ΔT between the two ends was measured by two pairs of T-type thermocouples connected to a thermometer (HH806AU,

OMEGA). ΔT was maintained to be less than 5 K by carefully controlling the power of the heater. After the steady state had been established, the apparent Seebeck coefficient S was calculated by equation $S = \Delta U / \Delta T$, subtracting the Seebeck coefficient of silver electrodes ($\sim 6 \mu\text{V/K}$). A prototype power generator was made by connecting 20 pieces of TE fibers (coated with platinum at both ends) in series by silver paste and wires. To evaluate its TE performance, the power generator was wrapped around a paper cup filled with hot water. The output voltage was measured as a function of the temperature difference between hot bottom and cold top of the cup. And the output power was evaluated by measuring the current flowing through and the voltage drop across a load resistor, which was connected with the generator in series.

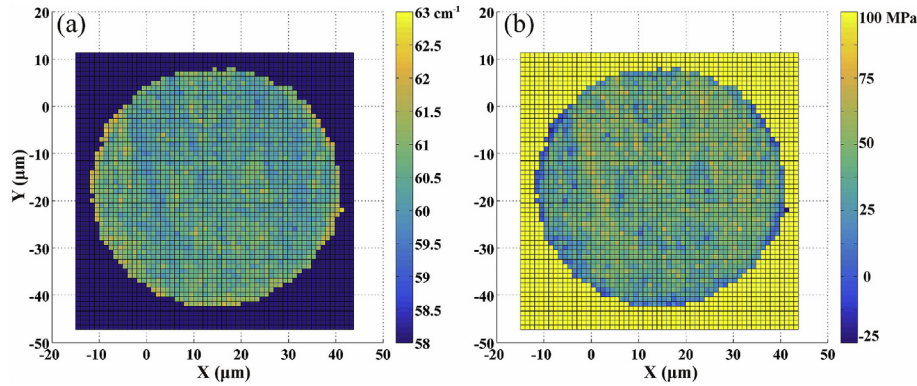


Fig. 5. Distribution maps of (a) Raman peak around 60 cm^{-1} and (b) stress values on the BF core.

3. Results and discussion

3.1. Compositional and structural characterization

To analysis the element distribution of ZF, KF, and BF fibers, three microchip samples at the core-clad interface were cut by FIB. The energy dispersive spectrometer (EDS) elemental mappings of these samples are exhibited in Fig. 1a–c, in which the left and right parts of the broken line denote the Bi_2Te_3 core and the glass cladding regions, respectively. As shown in Fig. 1a for the ZF fiber, there is little diffusion of Bi element into the cladding region. While, in Fig. 1b and c, there exist some Bi diffusions into glass cladding in about 100 nm and 500 nm depth for the KF and BF fiber, respectively. This should be attributed to higher drawing temperatures of the BF and KF fibers than that of ZF fiber. Nevertheless, only 500-nm-depth Bi diffusion should not seriously change the 40Bi–60Te proportion in the Bi_2Te_3 core of BF fiber for its relatively large core diameter ($50 \pm 5 \mu\text{m}$). Moreover, the composition in the ZF/KF/BF core was found to be ~40Bi–60Te mol.% by an electron probe microanalyzer (EPMA), as shown in Fig. S1 in the Supplementary Information.

Bi_2Te_3 cores were obtained by etching the as-drawn fibers in HF acid solution to strip glass cladding for X-ray diffractions (XRD) crystalline study. Fig. 2 shows the XRD patterns of the Bi_2Te_3 powder, rod, and three cores of ZF, KF, BF. It is obvious that all the diffraction peaks of the five samples can be indexed to the hexagonal Bi_2Te_3 crystalline phase (JCPDS No. 15–0863). Since the fiber underwent a quick cooling process during drawing fibers, the crystalline core should consist of polycrystals. The average size of Bi_2Te_3 polycrystalline particles in ZF, KF, and BF core was predicted to be nanoscale, when the XRD peak widths of ZF, KF, and BF core are broad and comparable to the peak widths of Bi_2Te_3 raw material with an average grain diameter smaller than 100 nm.

It can be also observed in Fig. 2 that there exist differences in diffraction peak intensities among the Bi_2Te_3 powder, rod and three cores. These Bi_2Te_3 cores show stronger diffraction intensities at (0 0 1) crystal planes than those of the Bi_2Te_3 powder and rod. This indicates there exists, to a certain degree, a preferred orientation of polycrystalline particles in fiber cores. According to the Lotgering method [23], the crystalline orientation degree of the (0 0 1) *c*-plane is termed as *F*:

$$F = \frac{P - P_0}{1 - P_0} \quad (1)$$

$$P_0 = \frac{I_0(00l)}{\sum I_0(hkl)} \quad (2)$$

$$P = \frac{I(00l)}{\sum I(hkl)} \quad (3)$$

where *P* and *P*₀ are the ratios of the integrated intensities (*I*) of all (0 0 1) planes to those of all (*h k l*) planes for preferentially and randomly oriented samples, respectively. For a standard polycrystalline powder sample of JCPDS, the value of *F* is equal to 0. On the contrary, if a sample is absolute (0 0 1) oriented sample of a single crystal, *F* should be 1. It is calculated that *F*_{ZF}~0.58, *F*_{KF}~0.73, and *F*_{BF}~0.9. The results indicate that all the Bi_2Te_3 polycrystals in three cores have a preferred orientation, and the Bi_2Te_3 polycrystals in BF core possess the strongest preferred orientation.

The preferred orientation of those polycrystalline cores should involve stress effect in the composite fiber configuration. During drawing these fibers, the fibers coming out the drawing heater underwent quick cooling ($>150 \text{ }^\circ\text{C/s}$). The volume shrinkages of the core and the cladding are differential for their distinct thermal expansion properties. Table 1 shows the basic thermal properties of Bi_2Te_3 , ZF3 glass, K9 glass, and Pyrex3.3 glass. The thermal expansion coefficient of Bi_2Te_3 ($17 \times 10^{-6} \text{ K}^{-1}$) [24] at 300 K is approximately two times that of ZF3 glass ($8.8 \times 10^{-6} \text{ K}^{-1}$), three times that of K9 glass ($7 \times 10^{-6} \text{ K}^{-1}$), and five times that of Pyrex3.3 glass ($3.3 \times 10^{-6} \text{ K}^{-1}$). Therefore, it can be inferred that each Bi_2Te_3 core in these fibers should shrink faster than its corresponding glass cladding during melt cooling and crystallizing, making Bi_2Te_3 core crystallize under a tensile stress in the core-clad fiber structure.

Among ZF, KF, and BF fibers, the BF core should undergo the biggest tensile stress because of the greatest thermal expansion difference between the core and the cladding. Fig. 3a exhibits the scanning electron micrograph of the BF fiber cross-section. Fig. 3b is the high-magnification image of the blue marked area in Fig. 3a. It can be observed that there are many bright and dark parallel stripes of nanosheets in the fiber core and these nanosheets display an ordered distribution. Fig. 3c shows the atomic $\text{Te}^{(1)}\text{—Bi—Te}^{(2)}\text{—Bi—Te}^{(1)}$ quintuples of Bi_2Te_3 structure [22], in which $\text{Te}^{(1)}\text{—Te}^{(1)}$ is of van der Waals bond among layers and $\text{Te}^{(1)}\text{—Bi/Bi—Te}^{(2)}$ is of covalent bond in single layer. Logically, the direction of tensile stress is mostly vertical to the fiber axis, as shown in Fig. 3d. Thus, Bi_2Te_3 core should crystallize in a manner that weaker van der Waals bond direction parallels to the tensile stress, i. e. Bi_2Te_3 layers are more parallel to the fiber axis. This is beneficial to decrease the Gibbs free energy of the fiber system. In the three fibers, the BF core micrographs exhibit a better *c*-plane

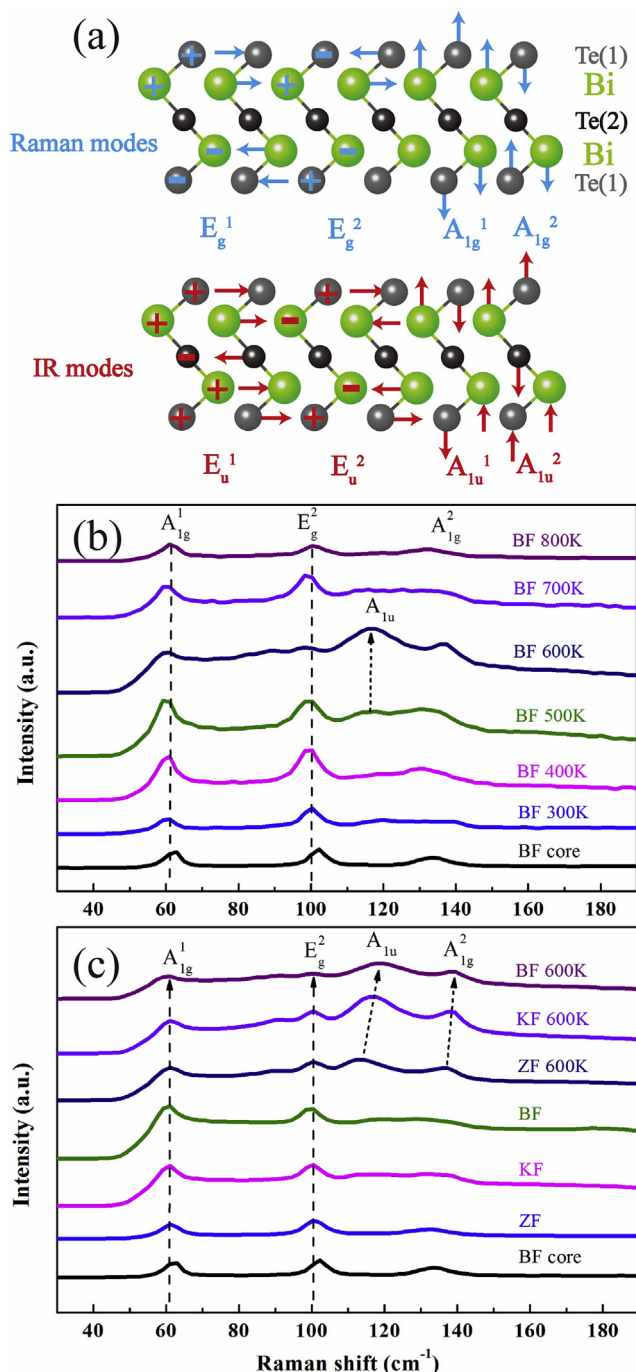


Fig. 6. (a) Schematic of the optical lattice vibrations in Bi_2Te_3 quintuples; (b) Raman spectra of the BF core annealed at 300–800 K and BF core without cladding; (c) Comparison among Raman spectra of BF core without cladding and three Bi_2Te_3 cores unannealed/annealed at 600 K.

orientation than ZF core and KF core, as shown in Fig. S2 in the Supplementary Information, which is consistent with the F values of orientation degree in the XRD patterns.

The sizes of nanosheets have been calculated based on the SEM data by using an image software and the results showed in the inset of Fig. 3b. For the BF core, most nanosheets are smaller than 25 nm, and the averaged thickness of single sheet is about 19 nm. In the same way, the averaged single-sheet thickness in the ZF and KF core is obtained to be 31 nm and 25 nm (Fig. S2 in the Supplementary

Information), being in accordance with the XRD patterns.

To analyze the microstructure of BF core with tension, a TEM test on the BF chip sample mentioned above was carried out and the related result is exhibited in Fig. 4. Fig. 4a presents a HAADF image of the BF chip sample. The left and right parts of the white broken line respectively denote the Bi_2Te_3 core and the glass cladding areas. In the core, there are many narrow stripes near the blue line selected area, stating an ordered structure in the BF core. And the selected area electron diffraction (SAED) pattern is shown in Fig. 4b, verifying that the Bi_2Te_3 core is in an ordered crystalline state and marking the corresponding lattice planes of (0 0 15) and (0 0 30). As Fig. 4c shows an HR-TEM image of the BF core, the core exhibits a crystal lattice spacing of ~ 1.01 nm, corresponding to interplanar spacing of the hexagonal Bi_2Te_3 (0 0 3) lattice plane. Fig. 4d shows an enlarged view of the boxed region in Fig. 4c and the atomic structure model of Bi_2Te_3 (0 1 0). The direction of Bi_2Te_3 (0 1 0) is parallel to the fiber axis.

3.2. Stress analysis

To characterize the stress in the BF core, as shown in Fig. 5a, a distribution map of Raman peak around 60 cm^{-1} was obtained on the BF fiber cross-section. Generally speaking for Bi_2Te_3 polycrystals, there is a sharp peak of $\sim 60\text{ cm}^{-1}$ in its Raman spectra [21]. And the peak will shift when Bi_2Te_3 polycrystals are under stress. Pressure stress makes the peak shift to a higher frequency and tensile stress makes it shift to a lower frequency, and the Raman frequency shift of Bi_2Te_3 polycrystals have a linear relationship with the stress value [25]. In Fig. 5a, the BF core exhibits Raman peaks distribution of $58\text{--}63\text{ cm}^{-1}$, marked in gradient color from blue to yellow. Then the effective Raman peak of the BF core distributes at a $50\text{-}\mu\text{m}$ -diameter circular region with a spatial resolution of $1\text{ }\mu\text{m}$. Commonly, Bi_2Te_3 Raman peak shift would be mainly affected by composition and stress [26]. In fact, the compositions in the ZF, KF, and BF core were found to be $\sim 40\text{Bi}\text{--}60\text{Te mol.}\%$ by EPMA, so the effect of composition change on these Raman peaks could be ignored. Herein, the Raman peak shift in the BF core mainly depends on stress. To estimate the stress value, the relationship between the stress value σ and the Raman peak frequency ω can be evaluated by a formula [25,27]:

$$\sigma = -26.3 \cdot (\omega - \omega_s) \quad (4)$$

where ω_s is the representative Raman peak position of Bi_2Te_3 single crystal without stress, i.e. 62 cm^{-1} at 300 K [25], based on the defect effect of stress on the Raman spectra [28]. According to this formula, a distribution map of the calculated stress values on the BF cross-section is displayed in Fig. 5b. The internal areas of the $50\text{-}\mu\text{m}$ -diameter core possess $0\text{--}+105.2$ MPa stress, meaning the inner core suffers a tensile stress. Then the average stress value in the inner core can be statisticised being 41.0 MPa. While the core-clad interface possesses $-26.3\text{--}0$ MPa stress, meaning the interface suffers a compressive stress. It is analogous to the stress distribution theory of reinforced glasses.

Fig. 6a displays the schematic of the optical-mode lattice vibrations in $-\text{Te}^{(1)}\text{--Bi--Te}^{(2)}\text{--Bi--Te}^{(1)}\text{--}$ quintuples [29]. There are fifteen lattice vibration modes in Bi_2Te_3 : three of which are three acoustic modes and twelve optical modes. According to the group theoretical classification [29], twelve optical modes include two A_{1g} , four E_g , two A_{1u} , and four E_u symmetry. Due to the inversion symmetry of the crystal, these optical modes are exclusively either Raman ($2A_{1g}$ and $4E_g$) or infrared ($2A_{1u}$ and $4E_u$) active. Both E_g and A_{1g} modes are twofold degenerate: the atoms in E_g vibrate in c basal plane, and the atoms in A_{1g} vibrate along c axis.

For obtaining the relationship between the stress and lattice

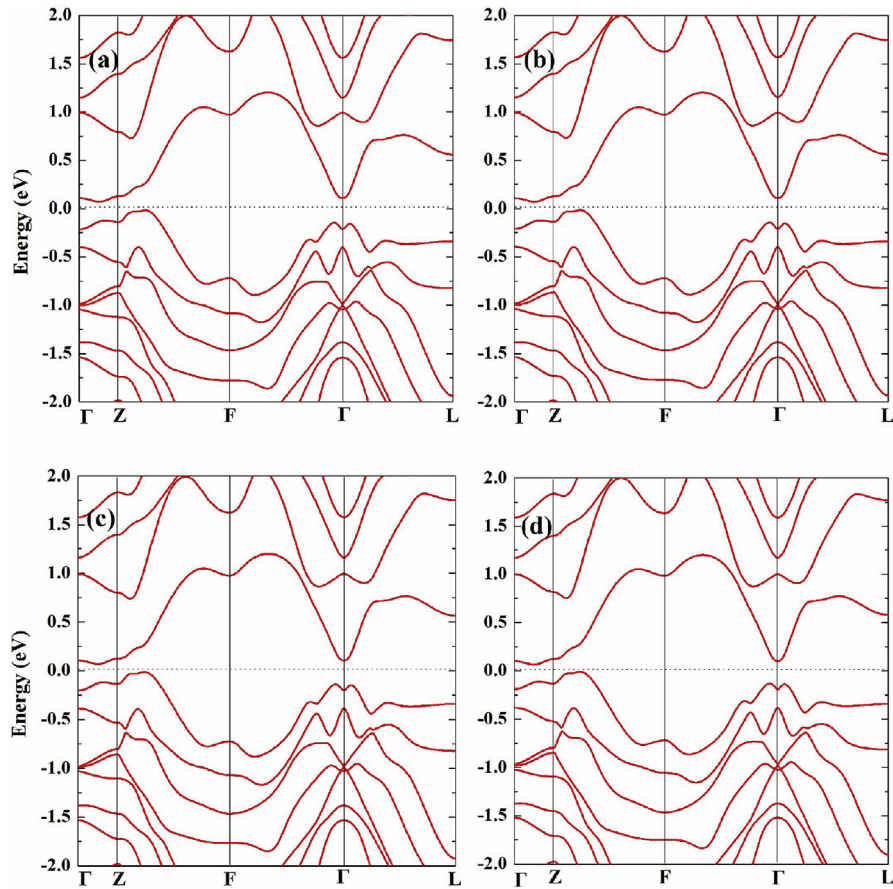


Fig. 7. Bi_2Te_3 band structure under (a) 0%, (b) 0.1%, (c) 0.3%, (d) 0.5% c -axis tensile strain.

vibrations in the fiber cores, the cores are annealed for 24 h at six temperature points from 300 K to 800 K respectively and one of the 800 K annealed cores is etched out by HF. Fig. 6b presents the Raman spectra on the samples of 24-h-annealed BF cores at 300–800 K with cladding and BF core annealed at 800 K without cladding. Due to the Raman peak around 60 cm^{-1} , it is observed that the core without cladding possesses a peak position of $\sim 62\text{ cm}^{-1}$, which is larger than other peak position and the same as the single crystal without stress [25]. It means this core is within almost zero stress, and then the treatment of annealing and etching could be applied in stress relieving. One more interesting thing is that there are main vibration peaks of A_{1g} , E_g , and E_u for all samples, but an additional peak appears at $\sim 117\text{ cm}^{-1}$ in the 500 K and 600 K annealed samples. There are two possible reasons could induce this additional peak. One is the change of Bi–Te elemental ratio after annealing, when Bi content is below 38 mol.% as reported in another literature [26]. The other is the specific lattice vibration in Bi_2Te_3 nanosheets [29]. However, the compositions in the ZF, KF, and BF core were all found to remain $\sim 40\text{Bi}-60\text{Te}$ mol.% by EPMA. Hence, this additional peak could be identified as the nanosheet lattice vibration in annealed Bi_2Te_3 core with less residual strain. It might be A_{1u} lattice-vibration mode composed of longitudinal optical phonons, and the A_{1u} -mode peak is infrared active in Bi_2Te_3 thin film but not in bulk Bi_2Te_3 [30]. The A_{1u} -mode peak appears in BF core samples with 500 K or 600 K annealing treatment can be attributed to crystal symmetry breaking between two interfaces

of single Bi_2Te_3 nanosheet [29]. Fig. 6c shows the Raman spectra comparison among the Bi_2Te_3 cores of unannealed and annealed ZF, KF, BF at 600 K A_{1u} -mode peaks can also be observed for the 600 K annealed ZF, KF, and BF cores, but not for other cores, and there is a blue shift of A_{1u} peak in the annealed cores from ZF to KF and BF. These confirm the lattice vibrations of Bi_2Te_3 quintuples would be affected by different tensile stress.

3.3. Band calculation

It has been confirmed that stress has strong influence on material band structure [10]. Since the Bi_2Te_3 core is too tiny to measure its energy band, the band structure of Bi_2Te_3 under c axis strain is calculated for simplification as its c axis strain should be greater than the a/b axis strain [31]. Next, the elastic constant (C_{33}) along c axis of Bi_2Te_3 is adopted being 47.7 GPa [31] and the average tensile stress value in the BF core are evaluated being 41.0 MPa as above, so the corresponding average tensile strain along c axis should be $\sim 0.09\%$. Next, 0%–0.5% c -axis tensile strain in Bi_2Te_3 is chosen for band calculation through first-principle calculations by using the Vienna Ab initio Simulation Package [32,33] based on the density functional theory [34]. The core-valence electron interactions are treated using the projector augmented-wave method [35]. The exchange-correlation potential is chosen as the generalized gradient approximation with the Perdew–Burke–Ernzerh (PBE) form [36]. A plane-wave basis set with a kinetic-energy cutoff of 320 eV is used. Spin-orbit coupling

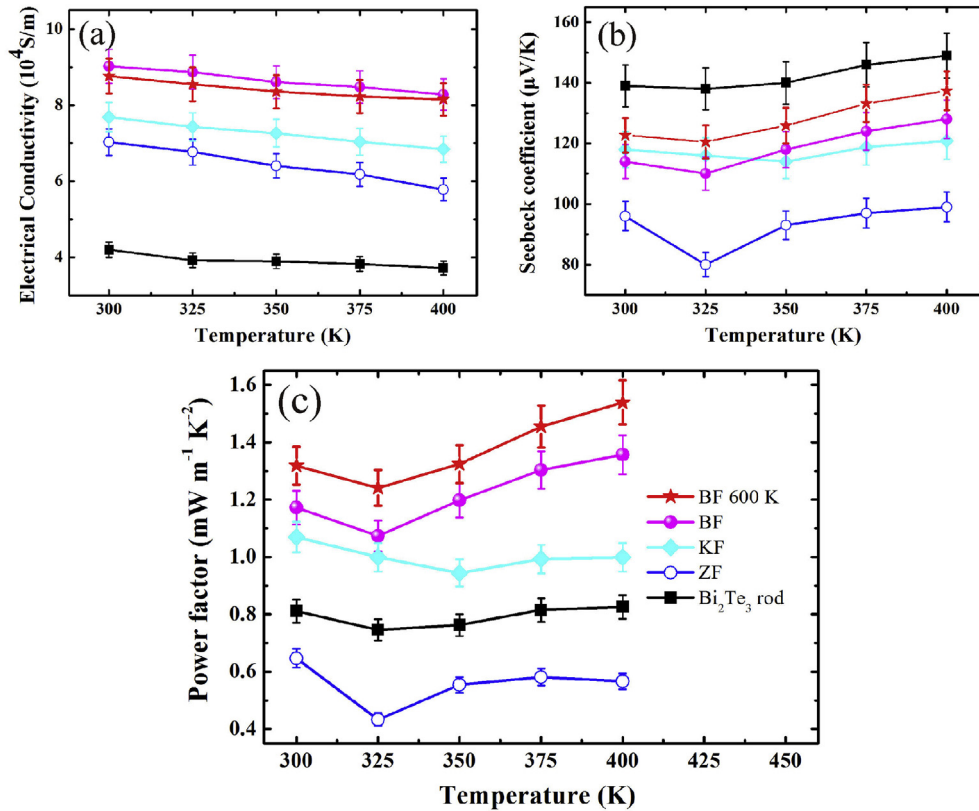


Fig. 8. (a) Electrical conductivities, (b) Seebeck coefficients, and (c) power factors of the Bi_2Te_3 rod and fiber core at 300–400 K.

Table 2

Electrical conductivities and Seebeck coefficients of the Bi_2Te_3 rod and the three Bi_2Te_3 cores with/without glass cladding at 300 K with 5% uncertainty.

Electrical properties	Bi_2Te_3 rod	ZF core	KF core	BF core	ZF core with cladding	KF core with cladding	BF core with cladding
σ (10^4 S/m)	4.19	5.21	5.4	6.82	7.02	7.68	9.02
S ($\mu\text{V}/\text{K}$)	139	114	128	125	96	118	114

(SOC) is considered and the default intensity parameters of SOC are applied. Finally, the band structures of Bi_2Te_3 with 0–5% tensile strain are calculated. Fig. 7 shows six band structures of Bi_2Te_3 under 0%, 0.1%, 0.3% and 0.5% tensile strain along c axis. Their indirect band gaps are calculated respectively being 0.086 eV, 0.085 eV, 0.082 eV and 0.075 eV, all of which are lower than a band-gap experimental value of 0.145 eV in Bi_2Te_3 without tensile strain [37]. Hence, the indirect band gaps of Bi_2Te_3 should decrease with the increasing c -axis tensile strain, and this result of the reductive band-gap trend states that Bi_2Te_3 under suitable tensile stress might tailor electrical transportation. And the density of state of Bi_2Te_3 under strain can be seen in Fig. S3 of the Supplementary Information. Compared with the pressure stress, it is more difficult to generate a tensile stress during melt crystallization. However, specific tensile stress can be introduced into our composite Bi_2Te_3 fibers for tailoring its band structure by the skillful use of the core-clad thermal expansion difference.

3.4. Thermoelectric properties characterization

Fig. 8 illustrates a pronounced difference in tensile behavior of electrical conductivities (σ), Seebeck coefficients (S), and power

factors (PF) among Bi_2Te_3 rod and fibers. Their electrical properties were tested by a same homemade setup as our previous study [38]. Fig. 8a presents the measured σ of the Bi_2Te_3 rod and cores at a temperature range of 300–400 K. All the σ values monotonously decrease with increasing temperature, exhibiting typical metallic-like electrical transport properties, which come from the well-known carrier-defect and carrier-phonon scattering effects [39]. All the σ are enhanced with increasing tensile stress and orientation degree, which order is Bi_2Te_3 rod–ZF–KF–BF 600 K–BF. The similar σ enhancement in oriented Sn–Se core fibers was discussed previously [38], declaring the tensile stress for tuning electrical transportation could be applied to various layered chalcogenides. Fig. 8b illuminates S of the Bi_2Te_3 rod and core at 300–400 K. The corresponding S decrease slowly almost with increasing tension, which order is rod–BF 600 K–KF–BF, except for the lowest S of the deformed ZF core (see Fig. S2a in the Supplementary Information). It was reported that improving orientation degree slightly reduced scattering factor and S [40]. For confirming that the Bi_2Te_3 cores possess a good stability, the electrical conductivities of as-drawn BF fibers are measured under 300–550 K (see Fig. S4 in the Supplementary Information). Further, as shown in Table 2, the electrical conductivities of every core without cladding are lower than that

with cladding, and the Seebeck coefficient of every core is higher than that with cladding. At the same time, the order of electrical conductivities maintains in ZF–KF–BF, which might arise from the maintaining oriented microstructure induced by tension before.

Fig. 8c displays PF of the Bi_2Te_3 rod and cores at 300–400 K. With applied tensile stress, the PF of samples at 400 K initially increases from $0.82 \text{ mW m}^{-1} \text{ K}^{-2}$ for the rod, to $1.0 \text{ mW m}^{-1} \text{ K}^{-2}$ for KF, and to $1.35 \text{ mW m}^{-1} \text{ K}^{-2}$ for BF. It can be attributed to the better orientation and larger carrier mobility in KF/BF than the rod [21]. The most interesting finding is that the 600 K-annealed BF core possesses the highest PF of $1.54 \text{ mW m}^{-1} \text{ K}^{-2}$ at 400 K. It should be attributed to the enhanced S after annealing for 24 h, because S might increase when the BF core tension was partly eliminated after annealing. Moreover, the annealed BF core has a power factor of $1.32 \text{ mW m}^{-1} \text{ K}^{-2}$ and a ZT value of ~ 0.76 at 300 K, when the thermal conductivity of the core is estimated being $\sim 0.52 \text{ W m}^{-1} \text{ K}^{-1}$ from our previous $89\text{-}\mu\text{m}$ -diameter Bi_2Te_3 fiber core [21]. For checking TE performance of the Bi_2Te_3 fibers, we prepare a daily paper cup covered with 20 pieces of BF fibers in series via silver electrodes, namely TE fiber cup generator, which can provide μW power under $\Delta T = 19 \text{ K}$ from waste heat of hot water (see Fig. S5 in the Supplementary Information). Hence, tuning tensile stress can be used to improve electrical transport in TE fibers and develop TE generators.

4. Conclusions

This study presented a simple method to fabricate the Bi_2Te_3 TE fibers with oriented nanosheet microstructure and outstanding electrical transportation. Rational tensile stress and annealing treatment can significantly enhance the power factor of the high-performance Bi_2Te_3 TE fibers. The resulting undoped Bi_2Te_3 cores exhibit a power factor of $1.32 \text{ mW m}^{-1} \text{ K}^{-2}$ and a ZT of ~ 0.76 at 300 K. And the TE fiber cup generator covered with Bi_2Te_3 TE fibers reaches a power of $0.47 \mu\text{W}$ under $\Delta T = 19 \text{ K}$. Tensile stress tuning from the physical mechanism of thermal size reduction can be an effective tool for the layered chalcogenide materials optimization at band structures and thermoelectric properties.

Declaration of competing interest

The authors declare that they have no known competing financial interests or personal relationships that could have appeared to influence the work reported in this paper.

Acknowledgements

This research was supported by Local Innovative and Research Teams Project of Guangdong Pearl River Talents Program (2017BT01X137); National Key Research and Development Program of China (2016YFB0402204); China Postdoctoral Science Foundation (2018M640777); Fundamental Research Funds for Central Universities (D2160590); National Natural Science Foundation of China (U1601205).

Appendix A. Supplementary data

Supplementary data to this article can be found online at <https://doi.org/10.1016/j.jmat.2020.02.004>.

References

- [1] Tritt TM. Holey and unholly semiconductors. *Science* 1999;283(5403):804–5.
- [2] Dresselhaus MS, Chen G, Tang MY, Yang RG, Lee H, Wang DZ, et al. New directions for low-dimensional thermoelectric materials. *Adv Mater* 2007;19(8):1043–53.
- [3] Hochbaum AI, Chen R, Delgado RD, Liang W, Garnett EC, Najarian M, et al. Enhanced thermoelectric performance of rough silicon nanowires. *Nature* 2008;451(7175):163.
- [4] Wright DA. Thermoelectric properties of bismuth telluride and its alloys. *Nature* 1958;181(4612):834.
- [5] Venkatasubramanian R, Siivola E, Colpitts T, O'Quinn B. Thin-film thermoelectric devices with high room-temperature figures of merit. *Nature* 2001;413(6856):597.
- [6] Tang X, Xie W, Li H, Zhao WY, Zhang QJ, Niino M. Preparation and thermoelectric transport properties of high-performance p-type Bi_2Te_3 with layered nanostructure. *Appl Phys Lett* 2007;90(1):012102.
- [7] Poudel B, Hao Q, Ma Y, Lan Y, Minnich A, Yu B, et al. High-thermoelectric performance of nanostructured bismuth antimony telluride bulk alloys. *Science* 2008;320(5876):634–8.
- [8] Huang HH, Lu MP, Chiu CH, Su LC, Liao CN, Huang JY, et al. Enhanced Seebeck coefficient of bismuth telluride compounds with graded doping profiles. *Appl Phys Lett* 2013;103(16):163903.
- [9] Choi H, Jeong K, Chae J, Park H, Baek J, Kim TH, et al. Enhancement in thermoelectric properties of Te-embedded Bi_2Te_3 by preferential phonon scattering in heterostructure interface. *Nano Energy* 2018;47:374–84.
- [10] Ovsyannikov SV, Shchennikov VV. High-pressure routes in the thermoelectricity or how one can improve a performance of thermoelectrics. *Chem Mater* 2009;22(3):635–47.
- [11] Morozova NV, Ovsyannikov SV, Korobeinikov IV, Karkin AE, Takarabe K, Mori Y, et al. Significant enhancement of thermoelectric properties and metallization of Al-doped Mg_2Si under pressure. *J Appl Phys* 2014;115(21):213705.
- [12] Ovsyannikov SV, Morozova NV, Korobeinikov IV, Lukyanova LN, Manakov AY, Likhacheva AY, et al. Enhanced power factor and high-pressure effects in $(\text{Bi,Sb})_2(\text{Te,Se})_3$ thermoelectrics. *Appl Phys Lett* 2015;106(14):143901.
- [13] Khvostantsev LG, Orlov AI, Abrikosov NK, Ivanova LD. Thermoelectric properties and phase transition in Sb_2Te_3 under hydrostatic pressure up to 9 GPa. *Phys Status Solidi A* 1980;58(1):37–40.
- [14] Polvani DA, Meng JF, Chandra NV, Sharp J, Badding JV. Large improvement in thermoelectric properties in pressure-tuned p-type $\text{Sb}_{1-x}\text{Bi}_x\text{Te}_3$. *Chem Mater* 2001;13(6):2068–71.
- [15] Jacobsen MK, Sinogeikin SV, Kumar RS, Cornelius AL. High pressure transport characteristics of Bi_2Te_3 , Sb_2Te_3 , and BiSbTe_3 . *J Phys Chem Solid* 2012;73(9):1154–8.
- [16] Brazhkin VV, Orlov AI. High-pressure thermoelectric characteristics of Bi_2Te_3 semiconductor with different charge carrier densities. *JETP Lett (Engl Transl)* 2014;99(5):283–5.
- [17] Atabaeva EY, Itskevich ES, Mashkov SA, Popova SP, Vereshchagin LF. Polymorphism of bismuth telluride at high pressures and temperatures. *Sov Phys Solid State* 1968;10:43.
- [18] Sakai N, Kajiwara T, Takemura K, Minomura S, Fujii Y. Pressure-induced phase transition in Sb_2Te_3 . *Solid State Commun* 1981;40(12):1045–7.
- [19] Polian A, Gauthier M, Souza SM, Triches DM, Cardoso LJ, Grandi TA. Two-dimensional pressure-induced electronic topological transition in Bi_2Te_3 . *Phys Rev B* 2011;83(11):113106.
- [20] Serebryanaya N, Tatyana E, Buga S, Kruglov I, Lvova N, Blank V. Monoclinic structure and electrical properties of metastable Sb_2Te_3 and $\text{Bi}_4\text{Sb}_{16}\text{Te}_3$ phases. *Phys Status Solidi B* 2015;252(2):267–73.
- [21] Sun M, Qian Q, Tang G, Liu W, Qian G, Shi Z, et al. Enhanced thermoelectric properties of polycrystalline Bi_2Te_3 core fibers with preferentially oriented nanosheets. *Appl Mater* 2018;6(3):036103.
- [22] Eibl O, Nielsch K, Peranio N, Volklein F. Thermoelectric Bi_2Te_3 nanomaterials. John Wiley & Sons; 2015.
- [23] Kobayashi T, Ogawa R, Miyazawa K, Kuwabara M. Fabrication of $\beta\text{-BaBi}_2\text{O}_4$ thin films with (001) preferred orientation through the chemical solution deposition technique. *J Mater Res* 2002;17(4):844–51.
- [24] Shiota I, Kohri H, Kato M, Ohsug JJ. Fine Bi_2Te_3 wires fabricated by glass sealed melt spinning. 25th International Conference on Thermoelectrics. New York: IEEE; 2006. p. 247–51.
- [25] Kullmann W, Geurts J, Richter W, Lehner N, Rauh H, Steigenberger U, et al. Effect of hydrostatic and uniaxial pressure on structural properties and Raman active lattice vibrations in Bi_2Te_3 . *Phys Status Solidi B* 1984;125(1):131–8.
- [26] Russo V, Bailiini A, Zamboni M, Passoni M, Conti C, Casari CS, et al. Raman spectroscopy of Bi-Te thin films. *J Raman Spectrosc* 2008;39(2):205–10.
- [27] Anastassakis E, Liarakis E. Polycrystalline Si under strain: elastic and lattice-dynamical considerations. *J Appl Phys* 1987;62(8):3346–52.
- [28] Zhao Z, Xue F, Mao Y, Chen N, Wang T. Effects of annealing on the residual stresses distribution and the structural properties of Si core fiber. *Opt Fiber Technol* 2018;41:193–9.
- [29] Shahil KMF, Hossain MZ, Teweldebrhan D, Balandin AA. Crystal symmetry breaking in few-quintuple Bi_2Te_3 films: applications in nanometrology of topological insulators. *Appl Phys Lett* 2010;96(15):153103.
- [30] Wagner V, Dolling G, Powell BM, Landwehr G. Lattice vibrations of Bi_2Te_3 . *Phys Status Solidi B* 1978;85(1):311–7.
- [31] Huang B, Li G, Yang X, et al. Capturing anharmonic and anisotropic natures in the thermotics and mechanics of Bi_2Te_3 thermoelectric material through an accurate and efficient potential. *J Phys Appl Phys* 2019;52(42):425303.
- [32] Kresse G, Furthmüller J. Efficient iterative schemes for ab initio total-energy calculations using a plane-wave basis set. *Phys Rev B* 1996;54(16):11169.

- [33] Kresse G, Furthmüller J. Efficiency of ab-initio total energy calculations for metals and semiconductors using a plane-wave basis set. *Comput Mater Sci* 1996;6:15.
- [34] Kohn W, Sham LJ. Self-consistent equations including exchange and correlation effects. *Phys Rev Lett* 1965;140(4A):A1133.
- [35] Blöchl PE. Projector augmented-wave method. *Phys Rev B* 1994;50(24):17953.
- [36] Perdew JP, Burke K, Ernzerhof M. Generalized gradient approximation made simple. *Phys Rev Lett* 1996;77(18):3865.
- [37] Sehr R, Testardi LR. The optical properties of p-type Bi₂Te₃ Sb₂Te₃ alloys between 2–15 microns. *J Phys Chem Solid* 1962;23(9):1219–24.
- [38] Sun M, Tang G, Liu W, Qian G, Huang K, Chen D, et al. Sn-Se alloy core fibers. *J Alloys Compd* 2017;725:242–7.
- [39] Rowe DW. *Thermoelectric handbook-marco to nano*. CRC/Taylor&Francis; 2005.
- [40] Lotgering FK. Topotactical reactions with ferrimagnetic oxides having hexagonal crystal structures-I. *J Inorg Nucl Chem* 1959;9(2):113–23.



Qi Qian received the Ph.d degree from the South China University of Technology, Guangzhou, in 2008. He is currently a professor in the Institute of Optical Communication Materials and State Key Laboratory of Luminescent Materials and Devices. His current research focuses on thermoelectric materials and optical fiber materials.



Zhongmin Yang received the Ph.D. degree from the Wuhan University of Technology, Wuhan, in 2002. He is currently the dean of School of Physics and Optoelectronics in South China University of Technology, and a professor in the Institute of Optical Communication Materials and State Key Laboratory of Luminescent Materials and Devices. His current research interests include areas of thermoelectric materials, luminescent materials and laser physics.



Min Sun received the Ph.d degree from the South China University of Technology, Guangzhou, in 2018. He is currently a post doctor in the School of Physics and Optoelectronics and the State Key Laboratory of Luminescent Materials and Devices in South China University of Technology. His current research focuses on thermoelectric materials and composite fiber materials.